UNIVERSIDAD SAN FRANCISCO DE QUITO USFQ

Colegio de Posgrados

Testing the feasibility to measure wrong displaced vertices from Lee-Wick particle decays with CMS experiment open data

Proyecto de investigación

Jonathan Joel Sánchez Jácome

Edgar Fernando Carrera Jarrín, Ph.D.
Director de Trabajo de Titulación

Trabajo de titulación de posgrado presentado como requisito
para la obtención del título de Magister en Física

Quito, 16 de agosto de 2022

UNIVERSIDAD SAN FRANCISCO DE QUITO USFQ

COLEGIO DE POSGRADOS

HOJA DE APROBACIÓN DE TRABAJO DE TITULACIÓN

Testing the feasibility to measure wrong displaced vertices from Lee-Wick particle decays with CMS experiment open data

Jonathan Joel Sánchez Jácome

Nombre del Director del Programa:	Dario Niebieskikwiat
Título académico:	Philosophy Doctor
Director del programa de:	Maestría en Física

Nombre del Decano del colegio Académico:	Eduardo Alba
Título académico:	Philosophy Doctor
Decano del Colegio:	Ciencias e Ingenieria

Nombre del Decano del Colegio de Posgrados:	Hugo Burgos
Título académico:	Philosophy Doctor

Quito, agosto 2022

© **DERECHOS DE AUTOR**

Nombre del estudiante: Jonathan Joel Sánchez Jácome

Código de estudiante: 00320088

C.I.:   1723965198

Lugar y fecha: Quito, 16 de agosto de 2022.

ACLARACIÓN PARA PUBLICACIÓN

UNPUBLISHED DOCUMENT

AGRADECIMIENTOS

Me gustaría agradecer a todas y cada una de las personas que directa o indirectamente contribuyeron al desarrollo de esta tesis. Primero a mi madre, padre y hermanos por su apoyo durante toda mi carrera y maestría. Quiero también expresar mi gratitud gigante a Edgar Carrera que con su apoyo e ingenio fue un pilar fundamental para el desarrollo de esta tesis y para mi desarrollo personal también. A Santiago Paredes por toda su colaboración con las distintas necesidades que presento el proyecto. Al director de la maestría Darío Niebieskikwiat y la coordinadora Milagros Pinto por siempre prestar atención para hacer lo mejor de este programa de Maestría. Especial mención a la familia USFQ y Poli Grants - HUBI Project 17462 que han hecho posible este proyecto. Al revisor de este proyecto y docente, Ernesto Contreras, que con su carisma y conocimiento supo brindarme sus conocimientos y ayuda a este trabajo. Al resto del cuerpo docente, en especial a Carlos Marín y su contribución al departamento. A la directora del pregrado, Melissa Infusino, y el director de laboratorios, Cristian Luciani, que coordinaron nuestra estancia como docentes de tiempo parcial. A cada uno de mis compañeros de maestría, en especial a Julio César Andrade, Pablo Rúales y Diego Santana. A mi querido maestro y sensei Fernando Benavides siempre ha sido guía y ejemplo en mi vida. Al sensei José Vargas por su valiosa amistad y cariño incomparables. A todos los demás senseis y compañeros por su amistad y esfuerzo que siempre me impulsa a dar lo mejor. A mis más queridos amigos que siempre me han apoyado con su consejo y amistad. Y todos aquellos allegados que con su calidez también han sido participes.

Resumen

En este trabajo se estudia la posibilidad de identificar observables para procesos que emergen del modelo estándar de Lee Wick en datos abiertos de la Colaboración CMS. Se considera que el más probable es la producción de pares de electrones de Lee Wick con masa igual a 200 GeV. El proceso de simulación del evento y simulación del detector se realiza tambien para valores de masas iguales a 300 GeV, 400 GeV y 500 GeV. Se caracteriza la señal considerando que cada una de las partículas decae a un electrón y un par de jets formando un vértice erróneamente desplazado del lugar de colisión. También describimos el método utilizado para reconstruir vértices desplazados que contengan un electrón y dos jets. Ademas, definimos una cantidad que distingue vértices del modelo estándar con respecto a los estudiados. Llevamos a cabo una comparación entre vértices obtenidos con el modelo de Lee Wick con vértices reconstruidos con procesos del modelo estándar y datos de CMS obtenidos durante la corrida 1 del LHC.

Abstract

In this work, we describe the feasibility to identify processes emerging from the Lee Wick standard model with in the open data from CMS Collaboration. We found that the most likely is the pair production of Lee Wick electrons 200 GeV. The process of event simulation and detection simulation is also carried for mass values of 300 GeV, 400 GeV, and 500 GeV. The signal is characterized considering that each particle decays into an electron and a pair of jets, which form a wrong displaced vertex with respect to the point of collision. We detail the method used to reconstruct displaced vertices from one electron and two jets. We also define a quantity to distinguish vertices from the standard model and those from our signal. The resulting vertices from the Lee Wick model are compared to vertices reconstructed with standard model processes and the data obtained during LHC Run 1 in the CMS detector.

INDEX

Figure index

Table index

Chapter I

Introduction

1.1 Experimental features and data acquisition

1.1.1 Experimental features

The Large Hadron Collider (LHC) is the largest and most powerful particle accelerator in the world. It was built by the European Organization for Nuclear Research (CERN) and is located underground at the France-Switzerland border. It consists of two essentially circular beam pipes covered in magnets with a circumference of 27 Km. It is capable of accelerating and colliding bunches of protons up to energies in the order of TeV [1]. In each of the four collision points, large investigation centers collect data.

The Compact Moun Solenoid (CMS) is located in the collision point number 5 in the french side. It is a particle detector built around a big super-conducting solenoid magnet capable of generating 3.8 T magnetic field. This field is strong enough to bend trajectories of charged

particles produced during the collisions. Specialized sensors are located on the side and end-caps of a barrel shape. In the most inner part of the detector there are concentric layers of silicon tracker sensors. This sub-system detects particle trajectories (tracks) as they pass through almost unaffected. Surrounding the tracker system are the energy detectors: in the electromagnetic (EM) calorimeter, EM particles deposit their energy and in the hadronic calorimeter, hadrons do the same. For an schematic detail, see Figure 1.1. Further experimental details of the detector will be mentioned as needed or can be found elsewhere [2].
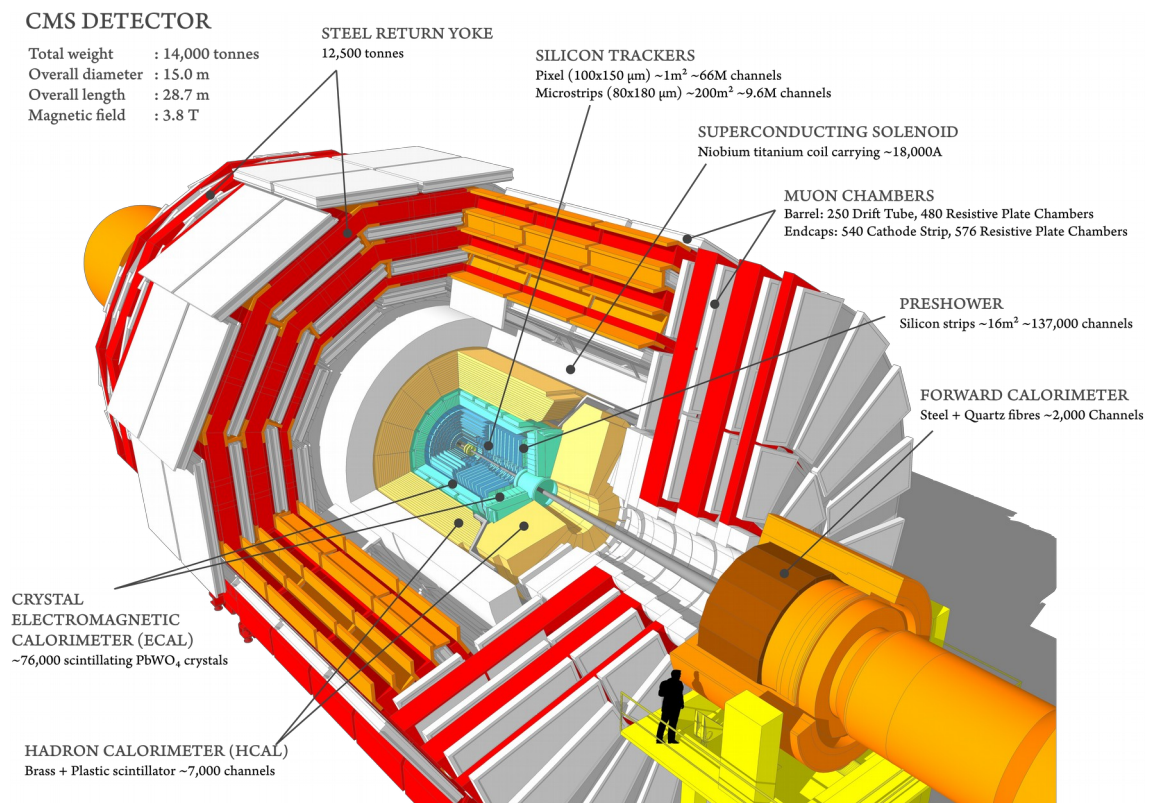
Figure 1.1: A perspective view of the CMS detector [2]

1.1.2   Data acquisition

The electronics at CMS limit the rate of processable data to 100 KHz.   However, during collision of bunches, events may be occurring at rates in the order of   GHz. For this reason, the experiment is forced to select the most interesting events to be processed and stored. This system, named Level-1 trigger, activates data acquisition if it finds energetic-enough particles or interesting topologies. These events are then sent to the high level trigger (HLT), which partially reconstruct the particles calorimeter and track information. This helps to select more interesting topologies and not to waste processing power in the most common events. This system is also capable of classifying events by their content [3]. The data are then processed and stored in the so-called AOD files. This is a format based on the analytic tool ROOT [4], a framework written in C++ specialized in the analysis of large amounts of data.

CMS has a pioneering and robust open data policy. Nowadays, it is possible to find public data taken until 2012, in the so called Run 1 of the LHC. These consist of several Petabytes of collision events and simulated datasets used in during studies of the Collaboration.   Similarly, the official CMS software (CMSSW) [5] and ROOT versions are available and constantly updated, so any user can replicate or make new analysis with the data.

1.2   Theoretical framework

Causality is a fundamental cause-effect principle characterized by the succession of two events. In most fundamental theories, such as special relativity, causality is mandatory to preserve Lorentz invariance. This relation of succession is necessary to describe the macroscopic world.

No violation of it has ever been observed. However, in the realm of fundamental interactions, as will be later discussed, the cause-effect succession may not be mandatory.

Beside the accuracy of standard model (SM) predictions, there are still unclear relations between theory and physical observations. For instance, the unlikely fine tuning requirements on the scalar sector, known as Hierarchy problem (HP), is a consequence of the divergences found in the loop order corrections of the SM [6]. This and other limitations have encouraged physicists to formulate diverse extensions of the SM that could solve these problems and explain the experimental observations more thoroughly.

The Lee-Wick standard model (LWSM)[7] is an extension of the SM. It is based on the finite theory of quantum electrodynamics model proposed by Lee and Wick [8]. This theory solves the HP with the addition of new massive Lee-Wick (LW) partner to each field in the SM. These fields are required to have negative eigenvalues on the metric for a given representation, in order to grant the unitarity of the scattering matrix. In consequence, LW-particles cannot be found in any asymptotic state, and any effect produced is restricted to the scale of the interaction [8].

Among other consequences, the theory predicts a measurable evidence of interactions mediated by LW-fields named as advancement of scattered waves [8]. This effect is similar but opposite to retarded scattering, implying that the measured wave front seem to exist before the scattering happened. The predicted scales of these advancements are too small in order to be considered measurable in prior experiments. Nowadays, the energetic proton-proton collisions occurring at the LHC could produce such events, and they might be observable by CMS and other experiments.

Interactions mediated by LW-particles are expected to behave as resonant decays [7]. Usually, after the creation of a resonance, it travels a characteristic distance λ, determined by the width Γ of the resonance, before decaying into its products. In the case of regular particles, these two events are causally related. On the other hand, LW-theory predicts that the products seem to appear before (or at the same time) the resonance is generated, as if the LW-particle traveled backwards in time [9]. Because of this, it would be possible to distinguish two geometrical places: the primary vertex (PV), where the initial collision occurs and the resonance is generated, and the secondary vertex (SV), where the decay happens. In causal decays, the displacement from PV to SV ($\overrightarrow{PV\,SV}$) is expected to be mostly parallel to the momentum of the resonance ($\vec{P}$), depicted in Figure 1.2a. This, however, is different in the case of LW-resonances, where the $\overrightarrow{PV\,SV}$ and $\vec{P}$ are antiparallel. This effect was denominated as wrong displaced vertex (WDV) [10], depicted in Figure 1.2b, and it is subject to be tested at the LHC.

Theory predicts that LW-leptons, with mass ranges of hundreds of GeV, are more likely to produce a measurable WDV at the LHC experiments. LW-bosons and LW-quarks with mass ranges above 3000 GeV, are too rare to be taken into account [10]. The best candidate to consider is the pair production of LW-electrons (PPLWE) ($\tilde{\ell}^e$) emerging from the neutral current (NC) sector of LWSM [10]:

$$\boldsymbol{L}_{NC} = -Z_\mu[g_Z^{e_L}(\bar{e}_L\gamma^\mu e_L - \bar{\tilde{\ell}}_{eL}\gamma^\mu \tilde{\ell}_{eL}) + g_Z^{e_R}(\bar{e}_R\gamma^\mu e_R - \bar{\tilde{\ell}}_{eR}\gamma^\mu \tilde{\ell}_{eR})$$
$$+ (g_Z^{e_L} - g_Z^{e_R})\frac{m_e}{M_\ell}(\bar{e}_R\gamma^\mu \tilde{\ell}_{eR} - \bar{\tilde{\ell}}_{eR}\gamma^\mu e_R)].$$

$$(1.1)$$

The NC sector contains the information for vertices with a Z boson and a pair lepton anti-lepton. The strength of this interactions depend on the electro-weak (EW) coupling constant

(a) Causal decay
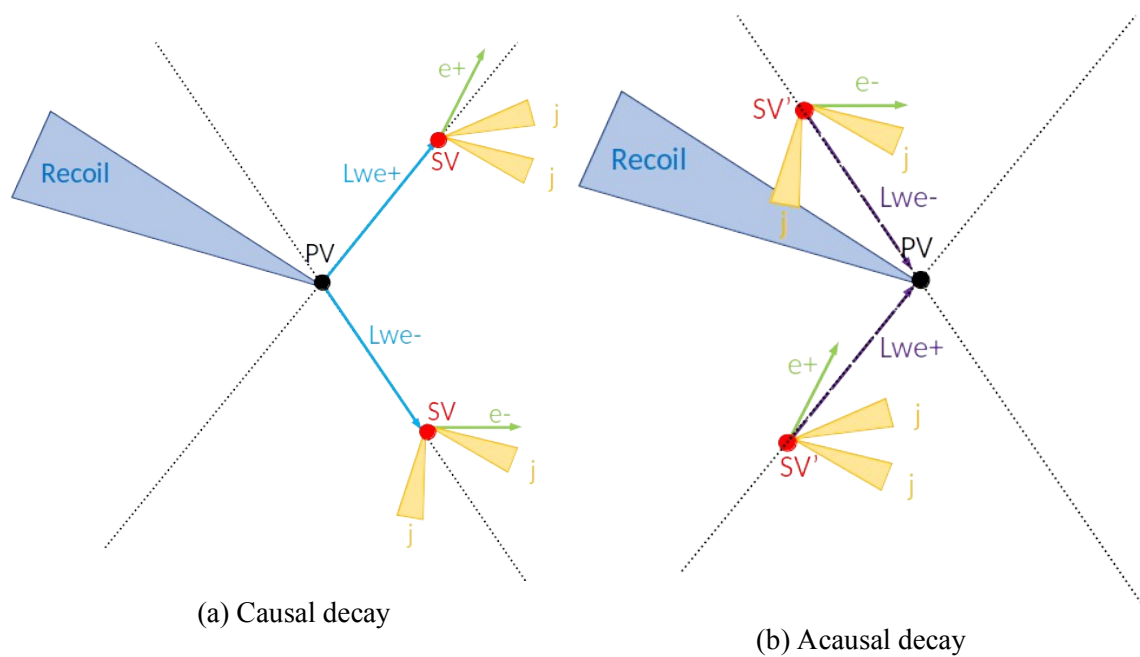
(b) Acausal decay

Figure 1.2: (1.2a) Resonant decay as if LW-electrons ($L_{we}\pm$) were produced in the primary vertex (PV) and causally decay at the secondary vertex (SV) into electrons ($e\pm$) and jets (j). (1.2b) Acausal resonant decay as if LW-electrons ($L_{we}\pm$) were produced in the PV and acausally decay at the wrong displaced secondary vertex ($SV^{'}$) into electrons ($e\pm$) and jets (j).

(EWCC) g_Z^e. In the first line of equation 1.1 are the terms related to the pair production of electrons and PPLWE for each parity. The PPLWE ($Z \to \ell^{e+}\ell^{e-}$) is proportional to the EWCC. In the second line we exhibit the most probable mixing term given by right-handed electrons and right handed LW-partners. Details for this calculations can be found in the appendices of reference [10]. This process is determined by EWCC g_Z^e, the electron mass m_e, and the mass of the LW-lepton M_ℓ. The final state ($\ell^+\ell^- \to e^+Ze^-Z$) gives a recognizable topology and could produce a measurable WDV [10].

1.3 Numerical calculation and simulation

The aim of this project was to study if the process $Z \to \ell^{e+}\ell^{e-} \to e^+Ze^-Z$ can be identified in CMS collaboration open data. To study this topology, we simulated the full model with similar conditions as those found at LHC in the so call Run 1. In it, bunches of protons were accelerated to 8 TeV and then collided. The CMS experiment is capable of reconsctructing, from tracks, the positions of PV and SV with a transversal precision Δx of approximately 0.02 mm [11]. If reconstructing a WDV is possible, it should happen that $\overrightarrow{PV\,SV} > \Delta x$. The magnitude of $\overrightarrow{PV\,SV}$ is exponentially distributed with mean in λ. Explicitly, we required $\lambda = v_T\,\gamma\,\tau > \Delta x$ where γ and τ are the relativistic factor and lifetime of the particle, respectively. In terms of the width of the resonance Γ, it is possible to obtain the transversal momentum condition $P_T > M_\ell\Delta x\Gamma$ [10]. This momentum can determine if the WDV could be an observable or not.

The implementation of the model was carried out in four steps. During the first step, we obtained the Feynman Rules using a Mathematica [12] package, named FeynRules [13]. This software allows the numerical calculation of Feynman rules from the Lagrangian of the model. For our analysis, we included Eq. 1.1 into the SM NC sector. From here we obtained the in-

formation for $Z \rightarrow \ell^{e+}\ell^{e-}$ and $\ell^{e\pm} \rightarrow e^{\pm}Z$ interaction vertices. The model was implemented for mass values $M_\ell = 200, 300, 400, 500$ GeV. Details of this step in the simulation are in the Annex A.1.1.

For the second step, the obtained Feynman rules were implemented into the event simulator Madgraph [14]. With this software, we generated 150000 events of PPLWE from proton-proton collision at 8 TeV. Additionally, Madgraph calculates the cross-section (σ) and flight distances λ; these values may be found in Table 1.1. The produced events only contain the hard process of PPLWE. Notice that this λ value does not contain the relativistic correction, so particles may form a detectable WDV even if the value here is not bigger than Δx. Actually, the simplistic analysis described at the beginning of this chapter does not reflect the complexity of the vertex reconstruction. Details of it will be discussed in the next chapter. A full description of this stage in the simulation is found in Annex A.1.2.1.

Table 1.1: Calculated cross-section (σ) and fly distance (λ) for each mass value, $M_\ell = 200, 300, 400, 500$ GeV.

M_ℓ(GeV)	σ fb^{-1}	λ (mm)
200	5.97	2.70765×10^{-2}
300	0.96	1.64300×10^{-2}
400	0.23	1.21212×10^{-2}
500	0.06	9.65243×10^{-3}

In the third step, we carried out a Monte-Carlo (MC) simulation with Pythia 8 [15]. This consisted of the so called showering process. Here we defined the decay channel $\ell^{e+}\ell^{e-} \rightarrow e^+Ze^-Z \rightarrow e^+e^- jjjj$ to allow our particles to decay as traveling bodies. We restricted the Z-bosons to exclusively decay into a pair of quarks that will later form jets (j) during the showering process. Because Pythia makes sure that regular conservation laws are fulfilled, we can only

simulate LW-electrons as causally decaying particles.   The solution for this problem will be discussed in the next chapter. Finally, in step four, we used CMSSW.5.3.X [5] to simulate the detection and reconstruction of particles as if they were sensed by the CMS experiment.   This file is stored in AOD-format.   Details of these two simulation steps are described in Annex A.1.3.1.

Chapter II

Analysis

2.1 Signal characterization

Similar to other resonances, it is no possible to detect LW-electrons directly. For that reason, we determined different signatures for its existence and, consequently, signatures for WDV. These results will later be compared to other simulated processes and to the actual experimental data. We were not able to actually fully characterize our topology, but this could most certainly be achieved with proper improvements in the method of identification. We utilized the CMSSW.5.3.32 version to carry out this analysis, and the self implemented tool ROOT.

2.1.1 Electron identification

For this analysis, we studied the stored information for particles from MC simulation, which will be named as gen-particles, and particles from detection simulation, which will be named as reco-particles. The type of reco-electrons that we studied are named GSF-electrons [16]. By

studying gen and reco-electrons distributions, it was found that over 99% of electrons emerging from the process $\ell^+\ell^- \to e^+e^- jjjj$ have a transverse momentum greater than 20 GeV, see Figure 2.1. When comparing the number of gen-electron and reco-electron, it was found that reconstruction efficiency is $>$99%. In a similar way, we identified that 98% of the time the most energetic reco-electron emerges from our signal. If there are 2 reco-electrons in the event, 92% of the time they are matched to electrons from the process. If there are 3 or more reco-electrons, 92% of the time an electron from our signal is matched either on the second or the third most energetic reco-electron.
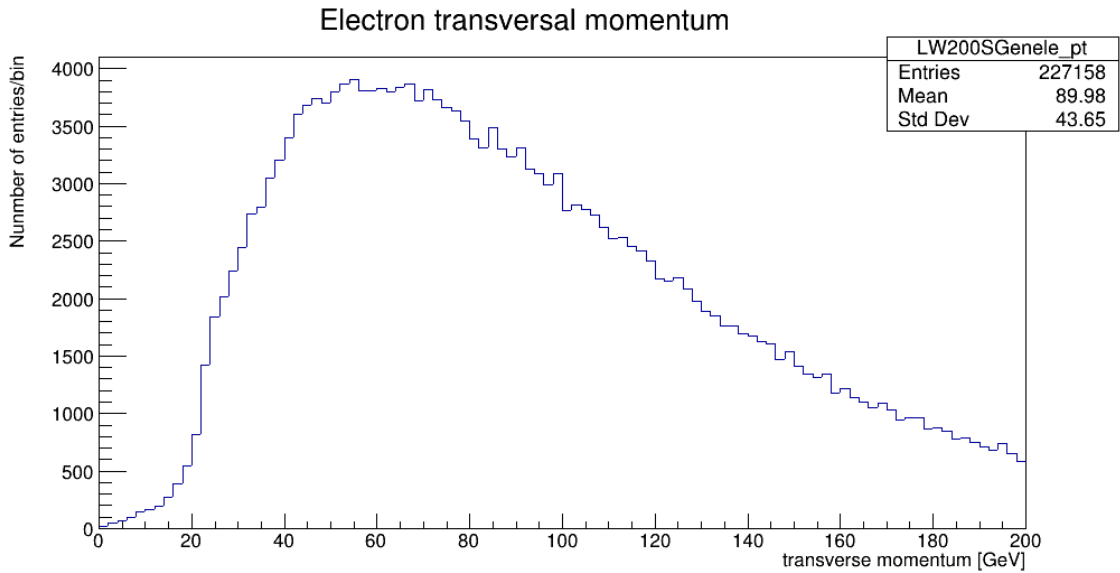
Figure 2.1: Transverse momentum distribution for gen-electrons emerging from process $\ell^+\ell^- \to e^+e^- jjjj$.

2.1.2 Jet identification

Jet identification was more challenging than electron identification, and it was not completed for this study. Jets are made of several particles that arrive to the detectors. For this reason, the

reconstruction and calibration for jets requires a most profound study out of the scope of this work [17]. We considered that gen-jet information comes from the first pair of particles generated (daugthers) from Z-boson decay. Reco-jets were obtained with the particle flow algorithm already implemented in CMS experiment [18]. These jets then are subject to an energy correction [17]. We discovered that jets from the process can not be identified to the most energetic reco-jets. Nonetheless, the Z-boson daughters (Z-daughters) should reconstruct an invariant mass M_{inv} approximately 91 GeV:

$$M_{inv} = \sqrt{(E_1 + E_2)^2 - (\vec{p}_1 + \vec{p}_2)^2}, \tag{2.1}$$

where $E_{1,2}$ are the energies of the particles and $\vec{p}_{1,2}$ their momenta. Because this distribution is imprecise it was deduced that the energy of reco-jets requires further calibration with a procedure not necessary for this work. However, 80% of reco-jets pairs emerging from the process have M_{inv} in range $80 - 160$ GeV. Notice that, if it would be possible to clearly identify the jets emerging from the process it would not be needed to do any further analysis for identification.

2.1.3 Electron-Jet properties

Up to this point, identification is insufficient to distinguish the signal from other processes. Nonetheless, the geometric properties between electrons and jets generated an efficient discriminant. The invariant mass between the electron and the pair of jets should reconstruct the mass M_ℓ, yet this has the same calibration problem from the previous subsection. Despite this, we found that due to the mass difference, the Z-boson carries most of the momentum from the LW-electron after the decay. This effect generated useful geometrical properties. For instance,

Reco-jet reconstructed invariant mass

LW200RecoZdauInvmass	
Entries	93498
Mean	119.1
Std Dev	23.88
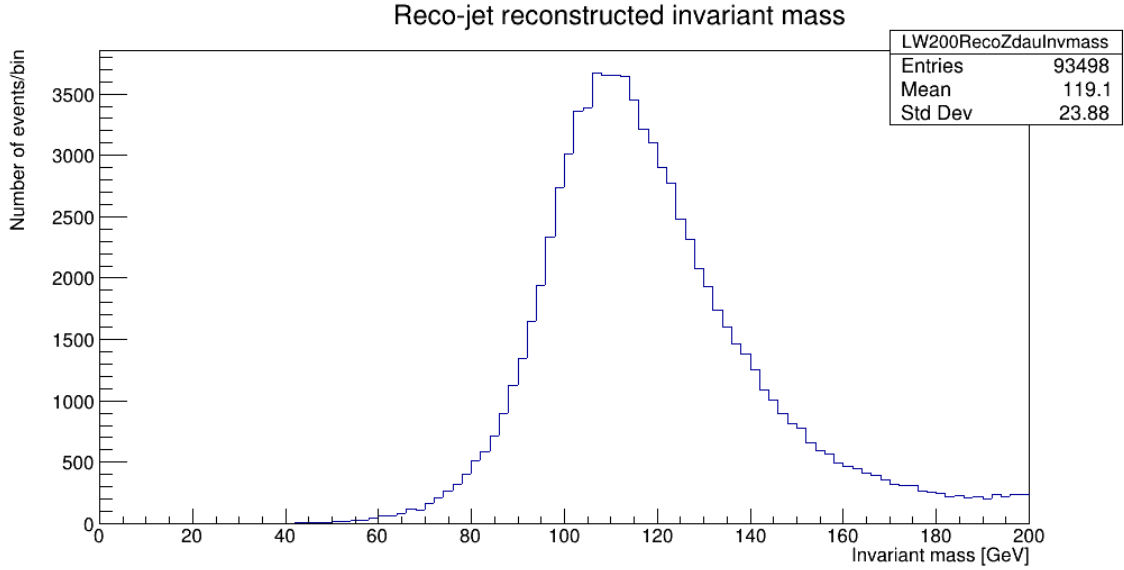
Figure 2.2: Invariant mass from pair of reco-jets emerging from process $\ell^+\ell^- \to e^+e^-jjjj$. The gen-jets are considered to be the first Z-daugthers.

let ΔR be the distance

$$\Delta R = \sqrt{\Delta\varphi^2 + \Delta\eta^2}, \tag{2.2}$$

defined by the difference in the azimuthal angles $\Delta\varphi$ and the pseudorapidities $\Delta\eta$ of two tracks. Then, the difference between ΔR_1 (distance: electron-closest jet) and ΔR_2 (distance:electron-second closest jet) obey the relation $|\Delta R_1 - \Delta R_2| < 0.2$, see Figure 2.3. This is most likely to happen in our topology; the explanation may be that all these objects emerge from the same vertex. For similar reasons we also found that a considerable number of jets posses an anomalous amount of EM energy. The reason being mixing between electrons and jets from the same vertex. As consequence, we restricted jets to electromagnetic energy fraction (EMEF < 0.6).
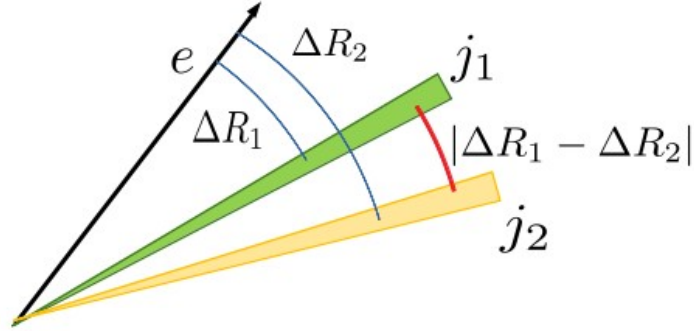
Figure 2.3: $|\Delta R_1 - \Delta R_2|$ defined as ΔR_1 (distance: electron-closest jet) and ΔR_2 (distance: electron-second closest jet, where ΔR is defined in Eq.2.2)

2.1.4   Vertex reconstruction

Displaced SV had already been reconstructed in previous works with CMSSW [19, 20, 21, 22]. Similar to those studies, we used the Kalman vertex fitting (KVF) algorithm. This can reconstruct SV from two or more tracks by fitting its point of maximum approach. The SV reconstruction algorithm (SVRA) we used is similar to that found in reference [23]. First, all possible pair of tracks with transversal momentum $p_t > 1$ GeV are subject to the KVF, and only those with Xi-squared normalized to the number of degrees of freedom $\chi^2_{norm} < 5$ are kept. Next, if it happens that two vertices share one or more tracks, they are refitted to a new SV with KVF. If the new vertex has $\chi^2_{norm} < 5$ and is geometrically compatible with the previous vertices, it is preserved, if not the two previous vertices remain. The merging of vertices is repeated iteratively until none of the vertices share tracks. Finally, the vertices are selected to criteria found in Table 2.1

By comparing gen-vertices and reco-vertices, we found that this method was great in obtaining an accurate position for the SV. Nonetheless, we did not make use of this method because it was hard to exclusively identify any pair of jets to each vertex. We found that the constituents of

Secondary vertices selection
Composed of at least 5 tracks
At least 3 tracks energy greater than 3 GeV
At least 2 tracks with $\Delta R < 0.4$, guaranties components from the same jet
At least 2 tracks with $\Delta R > 1.2$, guaranties components from different jets
$\Delta R > 4$ among all tracks prevent too much spreading

Table 2.1: Selection criteria from the secondary vertex reconstruction algorithm.

the vertex contain tracks from more than two jets. To prevent this problem, we implemented the SVRA to work on smaller set of tracks. This set of tracks consists of the combination between a singular electron and pair of jets. The resulting SV are then selected with the same criteria described in Table 2.1.

With the first described method we could identify our vertex by looking for the presence of an electron from the process. On the other hand, with the second method we obtained a number of SV candidates given by the combination of the electron and the pairs of jets. This limitation could be overcome if jets could be identified from the topology and, even more, if the position is contrasted with respect to the first method. This, however, will require an exhaustive analysis out of the scope of this project.

In spite of that, we chose the second method because we could define, for the first time, the quantity named parallelity of the SV ($\kappa_{\|} = \overline{PV}\,\overline{SV}^T \cdot \vec{p^T}$). As may be inferred, paralellity is a great signature in terms of acausality identification. The reason is that parallelity is expected to be positive when the SV is originated from a causal decay ($\kappa_{\|} > 0$); and negative when it is a WDV ($\kappa_{\|} < 0$). In our case, since we could not simulate acausal decays, it is matter to artificially choose the opposite sign of $\kappa_{\|}$ when the SV contains an electron from the process.

This may give rise to SV miss-identification because each electron is associated to more than one SV. A profound analysis of this is stated further in this manuscript.

2.2   Background, Data and trigger selection

2.2.1   Background selection

Similar processes that could miss-match our topology are known as background process. The CMS collaboration has published several datasets of simulated process in the AOD format. At first glance, we looked for a final topology with one these characteristics: two energetic electrons, pairs of jets from hadronic origin, and displaced vertices made of jet and/or electron tracks. The selected background processes were: Drell-Yan (DY) [24], top quark pair production (TTbar) [25], and W-boson production in association with jets (WJets)[26, 27, 28]; corresponding to cross-sections of 3503.7, 225.2 and 1.75×10^{-1} pb, respectively. DY is one of the most important background with respect of electron plus jets content, depicted in Figure 2.4b. TTbar contains displaced SV conformed by jets, depicted in Figure 2.4c. WJets contains jets and leptons, yet this was the less important of the backgrounds, depicted in Figure 2.4c.

q ℓ^- q $\ell^\pm$ g t

Z/γ^* $W^\pm$

q' (a) DY with jets ℓ^+ $\bar{q}$ (b) WJets $\bar{\nu}_\ell$ q (c) TTbar with jets $\bar{t}$
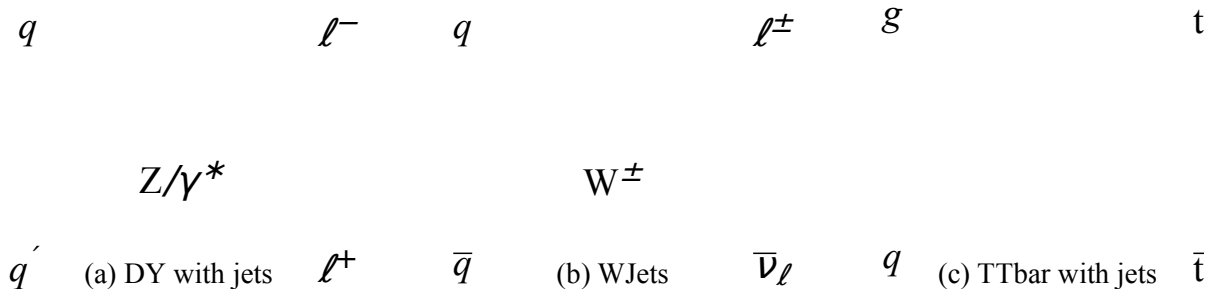
Figure 2.4: Feynman diagrams for the process: 2.4a Drell-Yan plus jets, 2.4c W-boson plus jets, and 2.4b Top-quark pair plus jets production.

2.2.2 Data and trigger selection

Many experimental data, in AOD format, from 2012, has already been made public by the CMS collaboration. They are classified by the content of the events. For instance, we selected the sets Double-Photon B [29] and C [30], with total integrated luminosity of 4412 and 7.055 fb^{-1}, respectively. These datasets are characterized by the presence of two energetic photon-like (egamma) particles. Similar sets, Double-Electron, characterized by the presence of electrons, were ignored because egamma-particles here are required to travel close to the PV, opposite to our topology. DoublePhoton, however, is less strict in the egamma selection. From the dataset, we selected the HLT triggers that better suited our analysis:

- HLT_Photon36_CaloId10_Iso50_Photon22_CaloId10_Iso50,

- HLT_Photon36_CaloId10_Iso50_Photon22_R9Id85,

- HLT_Photon36_R9Id85_Photon22_CaloId10_Iso50 and

- HLT_Photon36_R9Id85_Photon22_R9Id85.

These triggers guaranties the presence of two egamma depositions with transverse momentum p_t greater than 36 GeV and 22 GeV respectively. Additional features of the triggers refer to the showering shape and isolation of the egamma-particle deposition in the detectors.

2.2.3 QCD background

For simplicity, we expected that the addition of the backgrounds must fit the experimental data. This, however, did not happened because there are several QCD processes that were not considered. To estimate this contribution we defined a control region orthogonal to our topology. In those events the two most energetic egamma-particles selected by the trigger are required to

have the same charge. The QCD-background was then fitted to match experimental data and MC backgrounds in this region. The same fitting was extrapolated to the signal region. This prediction of the QCD-background worked successfully.

2.3   Event selection

Considering the criteria defined in Section 2.1, we selected the events of every set of data to better match our own topology. As general rule, the event yield for each step in the selection was found to be more efficient in our process. In the pre-selection, we required that all of our events pass any of the described triggers, at least have two electrons with $p > 20$ GeV and 4 jets with $p_t > 15$ GeV. This was the most general selection for our topology, and it filtered out most of the undesired data. Details of the event yield can be found in Table 2.2 under the acronym (TF). In the trigger object selection, with acronym (TO), we required that objects selected by the trigger to be reconstructed as GSF-electrons with $p > 40$ GeV and $p_t > 25$ GeV. This selection in p_t enhanced the efficiency of the triggers. In the cut with acronym (HQ), the track associated to our electrons must have fulfilled the high quality state described in references [22]. This is important when SV are reconstructed with electrons. Similarly, in (JetS), selected events must have contained at least 4 jets with the listed characteristics:

- Corrected transversal momenutm $p_t > 20$ GeV,

- Pesudorapidity $|\eta| < 2.5$,

- Number of constituents > 1,

- Neutral hadron energy fraction (NHEF) < 0.9,

- Neutral EM energy fraction (NEMEF) < 0.9,

Table 2.2: Number of events for each cut to simulated background and experimental data. *NF:* No filtered to data. *TF:* Data is selected to pass the trigger with two Egamma particles with $p_t > 36$ GeV and $p_t > 22$ GeV respectively. *TO:* Egamma-particles rare required to be electrons with $p_t > 40$ GeV and $p_t > 25$ GeV respectively. *HQ:* At least two electrons with high quality tracks. *JetS:* At least 4 jets to match quality checks and hadronic origin checks. *DRC:* Electron-jet structure is required to match $|\Delta R_1 - \Delta R_2| < 0.2$. *SG:* Data selected to have electrons with opposite charge. *IPP*: Require the presence of one good candidate for WDV in the data

Selection cut	DY	TTbar	WJets	QCD	LW200	LW300	LW400	LW500	Data
NF	40176928	2582368	96706945	-	67.7	11.0	2.6	0.7	66235981
TF	3953503.5	28237.1	46511.5	224649	51.2	9.2	2.3	0.6	5816590
TO	2005875	14889	15608	12140	28.8	5.7	1.5	0.4	2318120
HQ	1971623	14653	15297	9755	28.4	5.6	1.5	0.4	2251784
JetS	38282	3965	595	4721	11.4	2.3	0.6	0.2	69803
DRC	37547	3696	590	4768	10.7	2.2	0.6	0.2	68795
SG	31849	2740	330	1665	10.4	2.2	0.6	0.2	48857
IPP	10.6	22.5	2.5	55.1	0.02436	0.00440	0.00109	0.00030	144

- Muon energy fraction (MEF) < 0.8 and

- EMEF < 0.6.

Except for the last requirement, this selection matches that found in reference [23], where hadronic jets were selected to reconstruct SV. (DRC) selection refers to $|\Delta R_1 - \Delta R_2| < 0.2$ requirement in the electron-jet topology. (SG) is the event selection over electrons, we required they to have opposite charge. Notice that at this state the selected electrons are more exclusive category than the egamma particles consider in QCD-control region, so these two selections should not be mistaken to each other. Details of the event yield at each state of the selection may be found in Table 2.2.

In the final cut (IPP), events were selected requiring at least one SV to better match WDV topology:

- Is associated to an electron from the process,

- $\kappa_\parallel < 0$,

- Any other SV associated to the same electron have $|\overline{\overline{PV}}\,\overline{\overline{SV^T}}| > 0.02$ mm, and

- $|\vec{p^T}| > 20$ GeV.

One of the reasons for this selection comes from the results of the first SVRA, described in subsection 2.1.4. We found that $\kappa_\parallel$, for the signal process, was evenly distributed between negative and positive values. Initially, these values were obtained considering that $\vec{p^T}$ equals the addition of all transverse momenta from the tracks that fitted the SV. This indicates that tracks fitting the vertex came from different unclear sources. This was corroborated by comparing SV-tracks to jet-tracks with no clear co-relation between them. For this reason, we opted for the second method also described in the subsection 2.1.4. Even with this method, we found a symmetric distribution of $\kappa_\parallel$ values. The reason was that electrons were miss-combined with jet pairs to wrongly reconstruct a SV. This effect was found to be more frequent when the true SV transverse displacement was less than 0.02 mm. It also was found that if an electron emerging from a SV with displacement greater than 0 .02 mm its unlikely to generate poorly displaced vertices. After this selection, a 70% difference between correctly displaced and mismatched displaced vertices was observed in the LW-data. Additionally, the cut in $|\vec{p^T}| > 20$ GeV filtered out almost the totality of mismatched displaced vertices. The described asymmetry of $\kappa_\parallel$ at the SG stage can be appreciated in Figure 2.5. Even if $\kappa_\parallel$ values should all be negative, the asymmetry points that this investigation is on the right tracks. Better results could be achieved with improvements of the method such as the correct identification of the jets-electron-SV topology, as was stated in section 2.1.

Table 2.3: Systematic uncertainties for the selected objects that could mostly affect the value of parallelity calculation $\kappa_{\parallel}$

Source	Uncertainty(%)
Vertex reconstruction	18
Jet energy resolution	3
Electron energy resolution	1
Underlying event	3
Tracker misalignment	2
Integrated Luminosity	3
Trigger efficiency	1

2.4   Systematic uncertainties

The study for systematic uncertainties was not   carried out within the frame of this project. Nonetheless, we selected particles and events to better match literature, and so extrapolate its uncertainties. Trigger efficiency with TO selection is 99% [21].   Uncertainties in electron energy and tracking alignment are equal to 1% and 2% respectively.   These were inferred from a work with SV reconstruction with leptons [22].   The uncertainty in the jet energy resolution amounts to 3% and it was inferred from reference [17].   Vertex reconstruction uncertainty was estimated from a work with similar SVRA [23]. Because our methods are not exactly equal, we inflated the expected uncertainties to 18%. Uncertainties on integrated luminosity and underlying events are extracted from a work that uses the DoublePhoton dataset [21]. Detailed values for uncertainties are listed in Table 2.3.
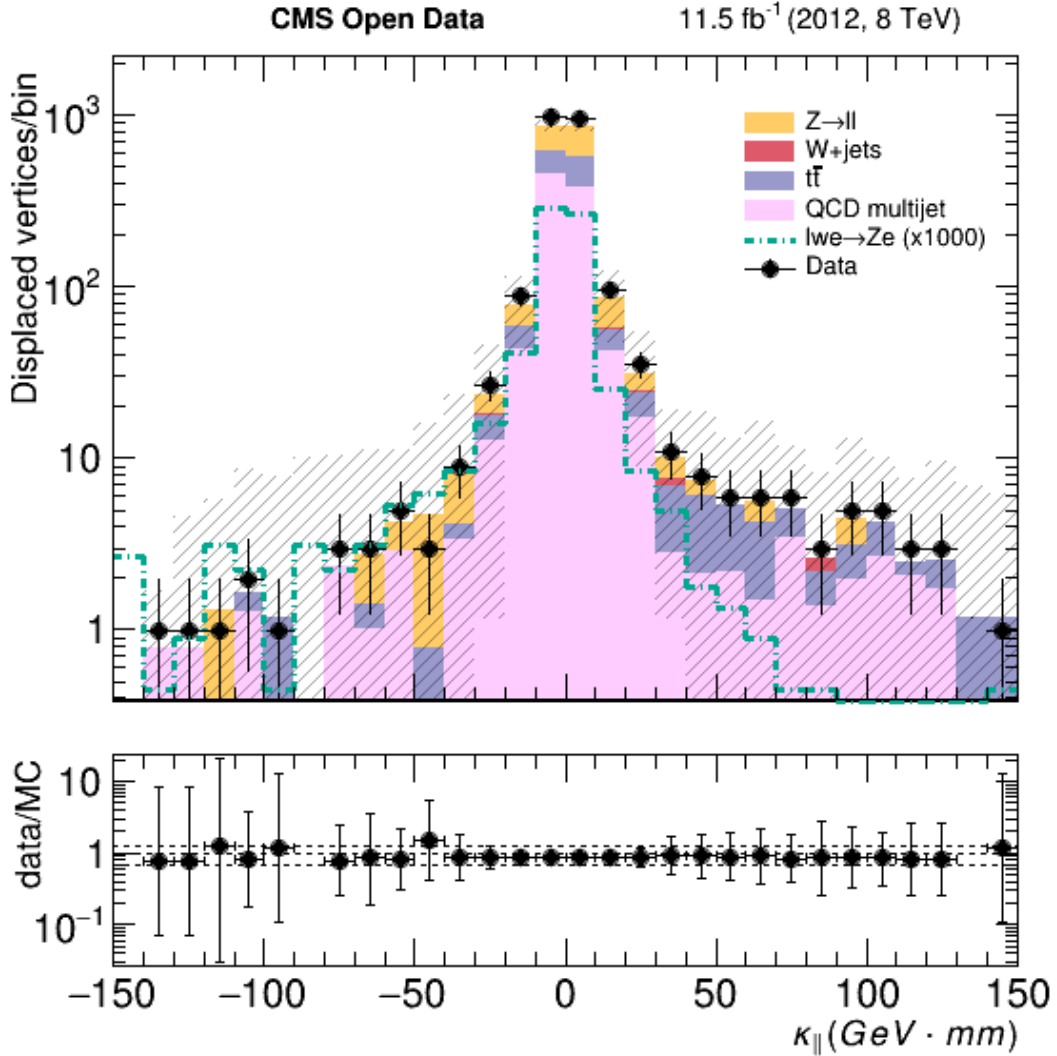
Figure 2.5: Histogram of parallelity $\kappa_{\parallel}$ calculated for each displaced vertex with transverse displacement greater than 0.02 mm and reconstructed from a pair of jets plus one electron. Black dots represent data acquired in CMS detector in Run 1, and the bars are its statistical uncertainty. Solid colors shown the background processes, and the hashed region is the calculated systematic uncertainty. The signal, scaled to 1000, is identified with a green dotted line, and it was obtained with LW-electron mass $M_{\ell} = 200$ GeV. The asymmetry between signal and background processes suggest the possibility to identify WDV.

Chapter III

CONCLUSIONS

In this work we tested the idea of measuring wave advancements predicted by Lee and Wick (LW) finite theories with the open data from the CMS Collaboration. This phenomenon, known as acausal decay, may be observed as a wrong displaced vertex (WDV). The most likely process that can produce such vertices is the pair production of LW-electrons. The event simulation of this process suggested that the mass of the LW-electron $M_\ell = 200$ GeV (with cross-section $\sigma = 5.97$ fb^{-1} and average flight distance $\lambda = 2.7 \times 10^{-2}$) was better fitted for this analysis, and most of the characterization of the signal was obtained from these data. The main reason was that we have to overcome the transversal spatial resolution ($\Delta x \approx 0.02$ mm) of the detector.

The characterization of the topology required the presence of two energetic electrons, 4 jets decaying from a pair of Z bosons, and 2 displaced secondary vertices (SV). About 98% of the time we were able to identify the most energetic electron in the data to the most energetic electron emerging from the process. The remaining electron was identified either to the second or third most energetic electron in the data with a 92% efficiency. The jets were not fully identi-

fied, but important signatures of its presence were obtained. For instance, 80% of the pair of jets from the process reconstructed an invariant mass within range 80 GeV $< M_{inv} <$ 160 GeV. Additionally, a mixture of electron and jets emerging from the same vertex was found. This jet-electron structure was not found in other background processes, and it is related to the inequality $|\Delta R_1 - \Delta R_2| <$ 0.2. SV obtained with the secondary vertex reconstruction algorithm (SVRA) using the total set of tracks are precise, yet this method lacks of clear jet identification. On the other hand, SV obtained with SVRA using the combination of tracks from electrons and paired jets generated a set of candidates for WDV. These candidates may be selected in the future by properly identifying the pair of jets from the process or by fitting it to most accurate reconstructed vertices. For the first time, we defined the quantity parallelity ($\kappa_{/\!/} = \overrightarrow{\overline{PV}\,\overline{SV^T}} \cdot \overrightarrow{P^T}$) that takes positive values for causal decays and negative values for acausal decays. With the described method, we were able to identify the $\kappa_{/\!/}$ values of a decay with certainty $>$ 60%. As result, we found that a small portion of the data may be considered to have a topology similar to LW-electron decay, yet more data will be needed to make any claim on this matter.

Although the topology was not fully characterized, we have shown that is possible to identify candidates of WDV from events containing a pair of energetic electrons and 4 jets in CMS open data. Furthermore, if its taken into account that LHC experiments will continue acquiring data with always improving technologies, the described method can be used to challenge the understanding of microscopic causality. This will require to expand the present study in the matter of topology identification and systematic uncertainties. Moreover, the concept of parallelity could be tuned up as a permanent system to detect WDV at LHC experiments.

References

[1] Lyndon Evans and Philip Bryant. "LHC Machine". In: *Journal of Instrumentation* 3.08 (2008), S08001–S08001. DOI: `10 . 1088 / 1748 - 0221 / 3 / 08 . S08001`. URL: `https://doi.org/10.1088/1748-0221/3/08/s08001`.

[2] S. Chatrchyan et al. "The CMS Experiment at the CERN LHC". In: *JINST* 3 (2008), S08004. DOI: `10.1088/1748-0221/3/08/S08004`.

[3] CMS collaboration et al. "The CMS trigger system". In: *arXiv preprint arXiv:1609.02366* (2016).

[4] Rene Brun and Fons Rademakers. "ROOT - An Object Oriented Data Analysis Framework". In: *AIHENP'96 Workshop, Lausane*. Vol. 389. 1996, pp. 81–86.

[5] CMS collaboration. *CMS Software Version 5_3_X (CMSSW_5_3_X)*. Version 2.3.X. 2016. DOI: `10.7483/OPENDATA.CMS.WYJG.FYK9`. URL: `https://github.com/cms-sw/cmssw/tree/CMSSW%5C_5%5C_3%5C_X`.

[6] Kurt Riesselmann. *Limitations of a Standard Model Higgs Boson*. 1997. DOI: `10.48550/ARXIV . HEP - PH / 9711456`. URL: `https : / / arxiv . org / abs / hep - ph / 9711456`.

[7] Benjamin Grinstein, Donal O'Connell, and Mark B. Wise. "The Lee-Wick standard model". In: *Phys. Rev. D* 77 (2008), p. 025012. DOI: `10 . 1103 / PhysRevD . 77 . 025012`. arXiv: `0704.1845 [hep-ph]`

[8] T. D. Lee and G. C. Wick. "Finite Theory of Quantum Electrodynamics". In: *Phys. Rev. D* 2 (6 1970), pp. 1033–1048. DOI: `10.1103/PhysRevD.2.1033`. URL: `https://link.aps.org/doi/10.1103/PhysRevD.2.1033`.

[9] Benjamín Grinstein, Donal O'Connell, and Mark B. Wise. "Causality as an emergent macroscopic phenomenon: The Lee-WickO(N)model". In: *Physical Review D* 79.10 (2009). ISSN: 1550-2368. DOI: `10.1103/physrevd.79.105019`. URL: `http://dx.doi.org/10.1103/PhysRevD.79.105019`.

[10] Ezequiel Alvarez et al. "Vertex Displacements for Acausal Particles: Testing the Lee-Wick Standard Model at the LHC". In: *JHEP* 10 (2009), p. 023DOI: `10.1088/1126-6708/2009/10/023`. arXiv: `0908.2446 [hep-ph]`

[11] Antonio Tropiano. *Tracking and vertexing performance in CMS*. Tech. rep. Geneva: CERN, 2012. URL: `https://cds.cern.ch/record/1603660`.

[12] Wolfram Research Inc. *Mathematica, Version 12.3.1*. Champaign, IL, 2021URL: `https://www.wolfram.com/mathematica`.

[13] Adam Alloul et al. "FeynRules 2.0 — A complete toolbox for tree-level phenomenology". In: *Computer Physics Communications* 185.8 (2014), pp. 2250–2300. ISSN: 0010-4655. DOI: `10.1016/j.cpc.2014.04.012`. URL: `http://dx.doi.org/10.1016/j.cpc.2014.04.012`.

[14] Johan Alwall et al. "MadGraph 5: going beyond". In: *Journal of High Energy Physics* 2011.6 (2011). ISSN: 1029-8479. DOI: `10.1007/jhep06(2011)128`. URL: `http://dx.doi.org/10.1007/JHEP06(2011)128`.

[15] Torbjörn Sjöstrand et al. "An introduction to PYTHIA 8.2". In: *Computer Physics Communications* 191 (2015), pp. 159–177. ISSN: 0010-4655. DOI: `10 . 1016 / j . cpc . 2015.01.024`. URL: `http://dx.doi.org/10.1016/j.cpc.2015.01.024`.

[16] W Adam et al. "Reconstruction of electrons with the Gaussian-sum filter in the CMS tracker at the LHC". In: *Journal of Physics G: Nuclear and Particle Physics* 31.9 (July 2005), N9–N20. DOI: `10.1088/0954-3899/31/9/n01`. URL: `https://doi.org/10.1088%2F0954-3899%2F31%2F9%2Fn01`.

[17] Vardan Khachatryan et al. "Jet energy scale and resolution in the CMS experiment in pp collisions at 8 TeV". In: (2017).

[18] Florian Beaudette. "The CMS particle flow algorithm". In: *arXiv preprint arXiv:1401.8155* (2014).

[19] Vardan Khachatryan et al. "Search for Displaced Supersymmetry in events with an electron and a muon with large impact parameters". In: *Phys. Rev. Lett.* 114.6 (2015), p. 061801. DOI: `10.1103/PhysRevLett.114.061801`. arXiv: `1409.4789 [hep-ex]`

[20] Serguei Chatrchyan et al. "Search for Top Squark and Higgsino Production using Diphoton Higgs Boson Decays". In: *Phys. Rev. Lett.* 112 (2014), p. 161802. DOI: `10.1103/PhysRevLett.112.161802`. arXiv: `1312.3310 [hep-ex]`

[21] CMS collaboration. "Evidence for a new state decaying into two photons in the search for the standard model Higgs boson in pp collisions". In: (2012).

[22]   Serguei Chatrchyan et al. "Search in Leptonic Channels for Heavy Resonances Decaying to Long-Lived Neutral Particles". In: *JHEP* 02 (2013), p. 085. DOI: `10 . 1007 / JHEP02(2013)085`. arXiv: `1211.2472 [hep-ex]`

[23]   Vardan Khachatryan et al. "Search for R-parity violating supersymmetry with displaced vertices in proton-proton collisions at $\sqrt{s}$ = 8 TeV". In: *Phys. Rev. D* 95.1 (2017), p. 012009. DOI: `10.1103/PhysRevD.95.012009`. arXiv: `1610.05133 [hep-ex]`

[24]   CMS collaboration. "Simulated dataset DYJetsToLL_M-50_TuneZ2Star_8TeV-madgraph-tarball in AODSIM format for 2012 collision data". In: *Open Data Portal* (2017). DOI: `10.7483/OPENDATA.CMS.ARKO.6NV3` . URL: `https://opendata.cern. ch/record/7730`.

[25]   CMS collaboration. "Simulated dataset TTbar_8TeV-Madspin_aMCatNLO-herwig in AODSIM format for 2012 collision data". In: *Open Data Portal* (2017). DOI: `10.7483/ OPENDATA.CMS.XH95.JNSE`. URL: `https://opendata.cern.ch/record/ 9518`.

[26]   CMS collaboration. "Simulated dataset W1JetsToLNu_TuneZ2Star_8TeV-madgraph in AODSIM format for 2012 collision data". In: *Open Data Portal* (2017). DOI: `10.7483/ OPENDATA . CMS . REHM ..` URL: `http : / / opendata . web . cern . ch record/9863`.

[27]   CMS collaboration. "Simulated dataset W2JetsToLNu_TuneZ2Star_8TeV-madgraph in AODSIM format for 2012 collision data". In: *Open Data Portal* (2017). DOI: `10.7483/ OPENDATA . CMS . DELK ..` URL: `http : / / opendata . web . cern . ch record/9864`.

[28] CMS collaboration. "Simulated dataset W3JetsToLNu_TuneZ2Star_8TeV-madgraph in AODSIM format for 2012 collision data". In: *Open Data Portal* (2017). DOI: `10.7483/ OPENDATA . CMS . HHCJ . TWKH`. URL: `http : / / opendata . web . cern . ch / record/9865`.

[29] CMS collaboration. "DoublePhoton primary dataset in AOD format from Run of 2012". In: *Open Data Portal* (2017). DOI: `10.7483/OPENDATA.CMS.CEPG.EXLP`. URL: `http://opendata.cern.ch/record/6005`.

[30] CMS collaboration. "DoublePhoton primary dataset in AOD format from Run of 2012". In: *Open Data Portal* (2017). DOI: `10.7483/OPENDATA.CMS.KT69.ANB8`. URL: `http://opendata.cern.ch/record/6031`.

[31] Céline Degrande et al. "UFO – The Universal FeynRules Output". In: *Computer Physics Communications* 183.6 (2012), pp. 1201–1214. DOI: `10.1016/j.cpc.2012.01. 022`. URL: `https://doi.org/10.1016%2Fj.cpc.2012.01.022`.

[32] J. Alwall et al. "A standard format for Les Houches Event Files". In: *Computer Physics Communications* 176.4 (2007), pp. 300–304. DOI: `10.1016/j.cpc.2006.11.010`. URL: `https://doi.org/10.1016%2Fj.cpc.2006.11.010`.

[33] Emanuele Usai Edgar Carrera Cesar Montero. *Examples for event generation with 2012 CMSSW machinery*. Available at `https://opendata.cern.ch/record/12052` (2022).

[34] G Petrucciani, A Rizzi, and C Vuosalo. "Mini-AOD: A New Analysis Data Format for CMS". In: *Journal of Physics: Conference Series* 664.7 (2015), p. 072052. DOI: `10. 1088/1742-6596/664/7/072052`. URL: `https://doi.org/10.1088%5C% 2F1742-6596%5C%2F664%5C%2F7%5C%2F072052`.

Anexos

Annex A

Simulation process

1.1 Feynman's Rules Calculation

In this section, there will be detailed information about the implementation in FeynRules and store the model in an UFO (Universal FeynRules Output) [31] package that will be later fed into MadGraph. All the described process should be done in the Feynrules directory.

The definition of the model is done by editing the file with extension `.fr`, which later will be fed into a notebook of Mathematica with extension `.nb`. There are previous loaded examples of how to define a model including a SM implementation in the in FeynRules subdirectory `Models`. We started by copying the `SM` directory, and renaming it as `LWSM`, we also renamed the file `SM.fr` as `LWSM.fr`. Implementation of LW-model for different values of M_ℓ can be found in our repository.

We will detail the followed steps to implement the model in the *LWSM.fr* file. In the Gauge-

Groups section, located at the top, are defined the gauge groups of the model. This part was not edited because we used the SM EW interactions. However, in any more complex approach of LWSM, gauge groups should defined for the new fields A.1. Indices section is unedited because we are using only one fermionic family, yet in this section we can define indexes for the other LW associated families. FeynRules uses the index information to unfold terms in the Lagrangian and/or tensorial operations A.2. In the InteractionOrderHierarchy (IOH) section, we did not change anything, yet this part is important since it tells Madgraph how to work with coupling constants. In our case, we take another solution for our couplings A.3. In ClassesDescription are located the definitions of particles. Each particle definition starts with the type (V for bosons, F for fermions, etc), and the index enclosed in brackets `[']'` which is unique for each particle. We only defined the LW doublet in the same way the electron doublet iss defined. We set `PDG -> 556`, which is exclusive for our particle. Here, it is important to change Width from `0` to `Auto` to allow this calculation based on the decays of the model. Notice that if set `Mass -> Auto` it will estimate the mass of the particles based on EW symmetry breaking (EWSB) A.4. In the parameters section are listed useful physical constants. It is possible to include new constants, but hierarchy of interaction must be declared in IOH section for each new constant A.5. This problem could be avoided by inserting the numeric factors directly in the Lagrangian. Details of the model constants for this investigation can be found in the appendices of reference [10]. Finally, we defined the Lagrangian from Eq. 1.1. We included every coupling constant by hand to avoid any conflict with the IOH and only included just the relevant mixing terms for our investigation. This one was added as a new term into the SM Lagrangian A.6. The resulting `.fr` files can be found in the simulation directory in the previously mentioned repository in the FeynRules directory.

In the `.nb` file, we executed Feynrules with lines the from the SM.nb file with the path to find the LWSM.fr file A.7. If the model is correctly implemented, it is possible to check vertices, widths, and write the UFO file. This is done using the WriteUFO command calling as seen bellow. The AddDecays flag was set in "True" mode, so Madgraph can use this information to calculate λ A.8. The result is a directory with the chosen name that contains all the relevant information of the model. This is ready to be used in Madgraph.

1.2   Matrix Element Calculator

1.2.1   Madgraph

We will detail the steps followed to generate events using Madgraph. We proceeded to copy the UFO directory in the `models` folder in the main directory of Madgraph (MDM). The program starts by typing in the console `./bin/mg5_aMC` when in MDM. Once the interface was running, we imported the model and checked if our vertices are well defined A.9. The next step is to generate the PPLWE of the event and write it out into a working directory A.10. Madgraph also allows us to add the decay channels with the process command, but we must not do that, since it will consider LW-electron decays as part of the hard process and not as traveling particles. The output command will create a directory inside MDM. This will be our working directory. In here is possible to check all the details of your event, such as Feynman diagrams, but also the managing cards for the simulation. In the `Cards` sub directory you can find the `param\_card.dat`, which contains information about physics of the particles. Here you must change the width `Wlwe` to `Auto`, this will allow Madgraph to calculated the width of our particle based in the info from the UFO model A.11. As result Madgraph rewrites this

card to contain all the calculated decays. This card also contains all the relevant properties of our particle that will be later needed to carry our Pythia step simulation A.12. We edited the `run\_card.dat` to set the energy of the beams to 4000 GeV (a total of 8TeV), same as in LHC run from 2012. In this card, we also defined the number of events that will be generated. In our case we simulated 15000 events A.13. Finally, we executed the calculation with the command `./bin/generate_events` when in `MDM/working_directory`. This step takes you to a confirmation screen that we bypassed to the calculation screens. In the first screen, make sure that the showering flag is off, do this because we are managing this part in the next step. You can on/off this option by typing 1. In the second screen, you can also edit the cards if you want to. Proceed by typing 0. Once finished, the output of the simulation will be an `unweighted\_events.lhe` file, which contains all the generated events, for details of the format refer to [32]. Additionally, we also obtained the cross section (σ) and the average flight distances (λ) for each point mass depicted in Table 1.1

1.3 Showering, detector and reconstruction

1.3.1 CMSSW, Pythia8

This part of the simulation was carried out in a CMSSW.5.3.32 [5] container. We used the preloaded cmsDriver tool, and the configuration comes from standard work [33]. This part is divided into three steps. The first part correspond to the Monte-Carlo (MC) simulation where the showering process is generated and stored in `.root` files. This requires to construct a sub-environment named as EdAnalyzer. This must be done in the `~/CMSSW_5_3_X/src` directory using bash commands A.14. Next we created the `MyHadronizer.py` file in the

python directory located in the EdAnalyzer `Sim directory`. This file contains all the configuration for the next steps A.15. In the `pythiaMyParameters` entry, we included the decay information extracted from A.12. Here the information was schemed according to particle data format from Pythia [15], that, among other information, includes λ for each particle. We set `isResonance=off` orders Pythia to generate displaced vertex based on λ value. In our case, we need the Z-boson(23) and LW-electron(556) to decay away from the primary vertex. We set `isVisible=off` so LW is not detectable. We also defined decay channels with `addChannel` A.15. To proceed, we included the previously generated `LWSM200DnR.lhe` file in the working directory and then invoked the cmsDriver command that generates the simulation files A.16. This is executed with `cmsRun gensimLW.py`. This will create the `gensimLW.root` file that contains the total of the MC simulation stored in CMSSW format.

In the next two steps we simulated the detection of the events as if they happened in cms-experiment. In the same directory of the previous step execute the HLT and RECO cmsDriver command A.17. Both of these commands must be executed in order with `cmsRun hltLW.py` then `cmsRun recoLW.py`. The result from the full simulation is stored in the AOD format [34].

Listing A.1: Feynrules gauge groups configuration.

```
M$GaugeGroups = {
  U1Y  == {
    Abelian          -> True,
    CouplingConstant -> g1,
    GaugeBoson       -> B,
    Charge           -> Y
  },
  SU2L == {
```

```
   Abelian            -> False,

   CouplingConstant  -> gw,

   GaugeBoson         -> Wi,

   StructureConstant -> Eps,

   Representations    -> {Ta,SU2D},

   Definitions        -> {Ta[a_,b_,c_]->PauliSigma[a,b,c]/2,

                          FSU2L[i_,j_,k_]:> I Eps[i,j,k]}
  },
  SU3C == {
   Abelian            -> False,

   CouplingConstant  -> gs,

   GaugeBoson         -> G,

   StructureConstant -> f,

   Representations    -> {T,Colour},

   SymmetricTensor   -> dSUN
  }
};
```

Listing A.2: Feynrules index configuration.

```
IndexRange[Index[SU2W      ]] = Unfold[Range[3]];

IndexRange[Index[SU2D      ]] = Unfold[Range[2]];

IndexRange[Index[Gluon     ]] = NoUnfold[Range[8]];

IndexRange[Index[Colour    ]] = NoUnfold[Range[3]];

IndexRange[Index[Generation]] = Range[3];


IndexStyle[SU2W,       j];

IndexStyle[SU2D,       k];

IndexStyle[Gluon,      a];

IndexStyle[Colour,     m];
```

```
IndexStyle[Generation, f];
```

Listing A.3: Feynrules IHO configuration

```
M$InteractionOrderHierarchy = {
  {QCD, 1},
  {QED, 2}
};
```

Listing A.4: Feynrules declaration of fermioninc field.

```
F[5] == {
      ClassName -> lwe,
      SelfConjugate -> False,
Indices -> {},
Mass -> {Mlwe, 200},
      Width -> Auto,
QuantumNumbers -> {Q -> -1, LeptonNumber -> 1},
PropagatorLabel -> lwe,
PropagatorType -> Straight,
      ParticleName -> "lwe-",
      AntiParticleName -> "lwe+",
PropagatorArrow -> Forward,
      PDG -> 556,
      FullName -> "LWElectron"},
```

Listing A.5: Feynrules coupling constants configuration.

```
  M$Parameters = {


   sw2 == {
```

```
    ParameterType -> Internal,
    Value          -> 1-(MW/MZ)^2,
    Description   -> "Squared Sin of the Weinberg angle"
  },
  ee == {
    ParameterType    -> Internal,
    Value            -> Sqrt[4 Pi aEW],
    InteractionOrder -> {QED,1},
    TeX              -> e,
    Description      -> "Electric coupling constant"
  },
  cw == {
    ParameterType -> Internal,
    Value         -> Sqrt[1-sw2],
    TeX           -> Subscript[c,w],
    Description   -> "Cosine of the Weinberg angle"
  },
  sw == {
    ParameterType -> Internal,
    Value         -> Sqrt[sw2],
    TeX           -> Subscript[s,w],
    Description   -> "Sine of the Weinberg angle"
  },
```

Listing A.6: Feyrules Lagrangian for LW-NC sector.

```
LLW := Z[mu] (-0.5+sw*sw)*ee/cw/sw lwebar.Ga[mu].ProjM.lwe +
  Z[mu] (sw)*ee/cw lwebar.Ga[mu].ProjP.lwe -
  (Z[mu]) (0.5)*ee/cw/sw*0.0005/200 (ebar.Ga[mu].ProjP.lwe
                              + lwebar.Ga[mu].ProjP.e) ;
```

```
LSM:= LGauge + LFermions + LHiggs + LYukawa + LGhost + LLW;
```

Listing A.7: Feynrules execution commands.

```
$FeynRulesPath = SetDirectory["...\\feynrules-current"]

<< FeynRules`

SetDirectory[$FeynRulesPath <> "/Models/LWSM"];

LoadModel["LWSM.fr"]

LoadRestriction["Massless.rst", "DiagonalCKM.rst"]
```

Listing A.8: Feynrules calculation commands.

```
vertsLW = FeynmanRules[LLW]

decays = ComputeWidths[vertsLW]

TWidthLW = TotWidth[lwe, decays]

bratio = BranchingRatio[{lwe, Z, e}, decays]

WriteUFO[LSM, AddDecays -> True, Output -> "LWSM200"]
```

Listing A.9: Madgraph model import and check.

```
MG5\_aMC> import model LWSM

MG5\_aMC> check lwe+ > e+ Z
```

Listing A.10: Madgraph event generation and store.

```
MG5\_aMC> generate p p > lwe+ lwe-

MG5\_aMC> output WorkingDirectoryName
```

Listing A.11: Madgraph `param_card.dat` definition of LW-electron.

```
###################################

## INFORMATION FOR DECAY
```

```
###################################
BLOCK QNUMBERS 556 #  lwe-
  1 -3 # 3 times electric charge
  2 2 # number of spin states (2s+1)
  3 1 # colour rep (1: singlet, 3: triplet, 8: octet)
  4 1 # particle/antiparticle distinction (0=own anti)
#*********
#     Decay widths       *
#*********
DECAY   6 1.508336e+00 # WT
DECAY  23 2.495200e+00 # WZ
DECAY  24 2.085000e+00 # WW
DECAY  25 4.070000e-03 # WH
DECAY 556 Auto         # Wlwe
```

Listing A.12: Madgraph rewritted `param_card.dat` definition of LW-electron.

```
###################################
## INFORMATION FOR DECAY
###################################
BLOCK QNUMBERS 556 #  lwe-
      1 -3 # 3 times electric charge
      2 2 # number of spin states (2s+1)
      3 1 # colour rep (1: singlet, 3: triplet, 8: octet)
      4 1 # particle/antiparticle distinction (0=own anti)
#*********
#     Decay widths       *
#*********
#     PDG        Width
DECAY  556   7.287748e-12
```

```
#  BR              NDA  ID1    ID2   ...
   1.000000e+00   2    23   11 # 7.287748021956571e-12
```

Listing A.13: Madgraph `run_card.dat` configuration.

```
15000 = nevents ! Number of unweighted events requested
0   = iseed   ! rnd seed (0=assigned automatically=default))


1          = lpp1    ! beam 1 type
1          = lpp2    ! beam 2 type
4000.0     = ebeam1  ! beam 1 total energy in GeV
4000.0     = ebeam2  ! beam 2 total energy in GeV
```

Listing A.14: CMSSW set environment.

```
cmsenv
mkdir SimLW; cd SimLW
mkedanlzr Sim; cd Sim
```

Listing A.15: Pythia8 and CMSSW configuration file.

```
import FWCore.ParameterSet.Config as cms

generator = cms.EDFilter("Pythia8HadronizerFilter",
   maxEventsToPrint = cms.untracked.int32(0),
   pythiaPylistVerbosity = cms.untracked.int32(1),
   filterEfficiency = cms.untracked.double(1.0),
   pythiaHepMCVerbosity = cms.untracked.bool(True),
   comEnergy = cms.double(8000.0),
   UseExternalGenerators = cms.untracked.bool(True),
   PythiaParameters = cms.PSet(
```

```
    processParameters = cms.vstring(
        'Tune:pp 5',
        'PDF:pSet = 5',
    ),


    pythiaMyParameters = cms.vstring(
      'LesHouches:setLifetime = 2',
      '556:new = lwe- lwe+ 2 -3 0 200.0 0.0 200.0
         200.0 2.70765e-02',
      '556:isResonance=off',
      '556:isVisible=off',
      '556:addChannel= 1 1.0 100 23 11',
      '23:isResonance=off',
      '23:oneChannel= 1   0.1540492    0      1      -1',
      '23:addChannel= 1   0.1194935    0      2      -2',
      '23:addChannel= 1   0.1540386    0      3      -3',
      '23:addChannel= 1   0.1193325    0      4      -4',
      '23:addChannel= 1   0.1523269    0      5      -5'
    ),


    parameterSets = cms.vstring('processParameters',
                                'pythiaMyParameters')
  )
)
```

Listing A.16: CMSSW command for simulation step.

```
cmsDriver.py SimLW/Sim/python/myHadronizer.py
--step GEN,SIM --datatier GEN-SIM
--conditions START53_V27::All
```

55

```
    --beamspot Realistic8TeVCollision

    --fileout gensimLW.root

    --customise Configuration/DataProcessing/Utils.addMonitoring

    --eventcontent RAWSIM --no_exec --filein file:LWSM.lhe

    --filetype LHE --number=10

    --python_filename gensimLW.py --mc
```

Listing A.17: CMSSW command lines for HLT and RECO step.

```
    # HLT
cmsDriver.py step1 --filein file:gensimLW.root

--fileout hltLW.root --pileup_input

root://eospublic.cern.ch//eos/opendata/cms/MonteCarlo2012

  /Summer12/MinBias_TuneZ2star_8TeV-pythia6/GEN-SIM

  /START50_V13-v3/0002/FEF2F4CC-0E6A-E111-96F6-0030487F1C57.root

--pileup 2012_Summer_50ns_PoissonOOTPU --datatier GEN-SIM-RAW

--conditions START53_V27::All --step DIGI,L1,DIGI2RAW,HLT:7E33v2

--mc --eventcontent RAWSIM --python_filename hltLW.py --no_exec

--customise Configuration/DataProcessing/Utils.addMonitoring

-n 10 --runsScenarioForMC Run2012_AB_C_D_oneRunPerEra


    # RECO
cmsDriver.py step2 --filein file:hltLW.root --fileout

recoLW.root --mc --eventcontent AODSIM,DQM --datatier AODSIM,DQM

--conditions START53_V27::All --python_filename recoLW.py

--no_exec --customise --step

RAW2DIGI,L1Reco,RECO,VALIDATION:validation_prod,DQM:

DQMOfflinePOGMC

Configuration/DataProcessing/Utils.addMonitoring -n 10
```